Effect of Impurity Ions on NBI Heating in LHD Plasmas*)

Hiroyuki YAMAGUCHI and Sadayoshi MURAKAMI

Department of Nuclear Engineering, Kyoto University, Nishikyo, Kyoto 615-8530, Japan

(Received 10 December 2013 / Accepted 17 April 2014)

The effect of impurity ions on NBI heating is numerically investigated in LHD plasmas. Helium and carbon are the two impurity species considered in the simulation. Fast-ion birth rates with various impurity fractions are calculated using the HFREYA code, taking into account ionization by the electron and ion impacts, and the charge exchanges with ions. The fast-ion birth rate is found to increase with increasing effective charge of plasma in the tangential injection NBI heating (beam energy: 180 keV) case, whereas the birth rate decreased in the perpendicular injection one (beam energy: 40 keV). The fast-ion slowing down is calculated using the GNET code, considering the Coulomb collisions with electrons, protons, and impurity ions. As the impurity fraction increases, the fast-ion confinement deteriorates because of the enhancement of the pitch-angle scatterings. Also, as the impurity fraction increases, the heat deposition per ion increases in the tangential injection NBI case and decreases in the perpendicular one.

Keywords: NBI heating, impurity, Large Helical Device, GNET

DOI: 10.1585/pfr.9.3403127

1. Introduction

In Large Helical Device (LHD), neutral beam injection (NBI) heating systems have been installed, greatly extending the temperature regime of LHD plasmas. In the high ion temperature (high-T_i) experiment [1, 2], ion temperatures up to 7.3 keV were achieved using NBI heating, with a total heating power of 25 MW. In these experiments, helium gas puffing and carbon pellet injection were carried out together with NBI heating; the the ion temperature increased during the decay phase of the electron density after the carbon pellet injection. The enhancement of neutral beam deposition in hydrogen plasma using carbon pellet injection in LHD has been reported [3]. However, a systematic study of the heat deposition of NBI heating with impurities is currently lacking.

In helical systems, the drift orbits of NBI fast ions are complex owing to the three-dimensional (3-D) effect of the magnetic configurations. We have developed the GNET code [4, 5] to study the confinement of the energetic particles and to evaluate the heat deposition profiles in the steady-state plasma of helical systems. We have also extended the GNET code to evaluate the heat deposition in the time-evolving plasma of the high-T_i experiment [6]. However, the effect of impurities was only considered in the slowing down calculation using a constant effective charge that was larger than unity. To accurately analyze the heat transport properties of the high-T_i plasma, it is necessary to evaluate the heat deposition profiles for each particle species including the effect of impurity ions on the Coulomb collisions.

In this study, we examine the effect of impurity ions on the heat deposition of NBI heating in LHD plasmas. There are two processes in the NBI heating. The first is the fast-ion birth process, in which the injected neutral beams from the injector are ionized in the plasma. The second is the slowing down process, in which the ionized fast ions drift in the plasma, and slow down towards the thermal velocity. We numerically simulated the two processes, considering the impurity effect on the ionization and the Coulomb collisions. In this study, we assume two impurity species: helium and carbon. We evaluate the dependence of the fast-ion distribution and the heat deposition on the impurity ion fraction. In section 2, we explain the simulation models of the fast-ion birth and slowing-down process. Next, the simulation results for the fast-ion birth and the heat deposition are discussed. Finally, we briefly summarize the conclusions.

2. Simulation Models

In the NBI heating system, accelerated neutral beams from the injector are ionized in the plasma and the ionized beams slow down to heat the plasma. We evaluate the fast-ion birth profile in LHD plasmas using the HFREYA code, which is a part of the FIT3D code [7]. The HFREYA code follows the trajectory of the fast neutrals injected from the beam injector into the plasma in 3-D real space, and calculates the ionization process using a Monte Carlo algorithm. The plasma geometry of the LHD plasma is introduced using the MHD equilibrium by the VMEC code.

The attenuation of the neutral beam flux $I(\boldsymbol{r})$ is expressed with

author's e-mail: yamaguchi@p-grp.nucleng.kyoto-u.ac.jp

*) This article is based on the presentation at the 23rd International Toki Conference (ITC23).

$$\frac{\mathrm{d}I(\boldsymbol{r})}{\mathrm{d}l} = -\sigma_s I(\boldsymbol{r}), \quad (1)$$

where l is the length along the beam line. We use the approximate form of the beam stopping cross-section σ_s in plasma with several of the impurity ion species proposed in ref. [8], where they considered the ionization of neutrals owing to electron impact, proton impact, impurity impact, and charge exchange with proton and impurity ions, including various excitation processes of neutrals.

Next, we evaluate the NBI fast-ion slowing down process using the GNET code [5], which can solve the drift kinetic equation in five-dimensional phase space (3-D in real and 2-D in velocity space), based on the Monte Carlo method:

$$\frac{\partial f}{\partial t} + (\boldsymbol{v}_\parallel + \boldsymbol{v}_\mathrm{D}) \cdot \nabla f + \dot{\boldsymbol{v}} \cdot \nabla_v f = C(f) + L + S, \quad (2)$$

where f is the fast-ion distribution function, $\boldsymbol{v}_\parallel$ is the velocity parallel to the field line, $\boldsymbol{v}_\mathrm{D}$ is the perpendicular drift velocity, $C(f)$ is the linear Coulomb collision operator, L is the particle loss term consisting of the orbit loss and charge exchange loss, and S is the particle source term calculated with the HFREYA code. We evaluate the fast-ion distribution in the phase space and the radial profile of the heat deposition, including the complex motion of the energetic fast-ions during their slowing down.

To consider the effect of impurity ions on the slowing down of the fast ions, we introduce the linear Coulomb collision operator for multi-species plasma as the sum of the operators for electrons, protons, and impurity ions:

$$C(f) = C_\mathrm{e}(f) + C_\mathrm{p}(f) + \sum_\mathrm{imp} C_\mathrm{imp}(f), \quad (3)$$

where the operators for each particle species follow ref. [9],

$$C_s(f) = \frac{\nu_d^s}{2}\frac{\partial}{\partial\lambda}(1-\lambda^2)\frac{\partial f}{\partial\lambda} + \frac{1}{v^2}\frac{\partial}{\partial v}\left[v^2\nu_E^s\left(vf + \frac{T_s}{m_b}\frac{\partial f}{\partial v}\right)\right], \quad (4)$$

where s is the particle species, $\lambda = v_\parallel/v$ is the cosine of the pitch angle, ν_d^s is the pitch angle scattering frequencies, ν_E^s is the energy scattering frequencies, T_s is the temperature, and m_b is the fast-ion mass, respectively.

3. Simulation Results

There are five NBI heating systems in the LHD: three tangential beam injectors with a negative ion source (#1 to #3) and two perpendicular injectors with a positive ion source (#4 and #5). We consider the two typical NBI heating systems of LHD: NBI#1 (tangential injection beam) and NBI#5 (perpendicular injection beam). The beam energies of NB#1 and NB#5 are set at 180 keV and 40 keV, respectively. In the NB#5 case with the positive ion source, the energy component of the fast ions (40 keV, 40/2 keV, and 40/3 keV) owing to the dissociation of molecular ions is taken into account.

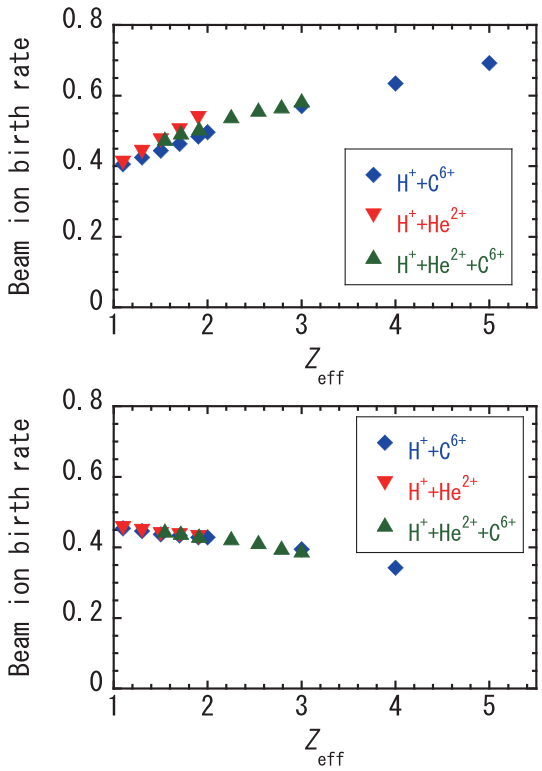

Fig. 1 Fast-ion birth rate as a function of the effective charge in the tangential injection case (top) and the perpendicular injection case (bottom).

We assume a magnetic configuration of R_ax = 3.6 m in LHD and the magnetic field strength at the center is B_0 = 2.75 T. The radial profiles of the electron density and electron temperature of the background plasma are fixed at $n_\mathrm{e}(\rho) = (1 - 0.9 \times \rho^8) \times 10^{19}$ m^{-3} and $T_\mathrm{e}(\rho) = 3 - 2.7\rho^2$ keV, respectively, where ρ is the normalized minor radius. We also set the temperature of each ion species to the same value as the electron temperature. Moreover, we set the radial density profiles of each ion species to be identical with the electron density profile. He^{2+} and C^{6+} ions are the impurity species. We perform the simulation changing the fraction of He^{2+} and C^{6+} ions. For the mixtures of He^{2+} and C^{6+} the helium charge density is set equal to the hydrogen charge density, and only the carbon fraction is varied.

First, we investigate the impurity effect on the fast-ion birth. Figure 1 shows the fast-ion birth rate as a function of the effective charge Z_eff, where $Z_\mathrm{eff} = \sum_j Z_j^2 n_j / \sum_j Z_j n_j$ and j denotes the ion species. We defined the fast ion birth rate as $(N_\mathrm{n} - N_\mathrm{shine})/N_\mathrm{n}$, where N_n and N_shine are the number of total injected neutrals and the number of neutrals that reached the wall of the opposite side (shine-through loss number), respectively. As Z_eff increased, the birth rate increases for the NBI#1 beams, whereas it decreases for the NBI#5 beams. This is a consequence of the beam energy dependence of the charge exchange cross section. The

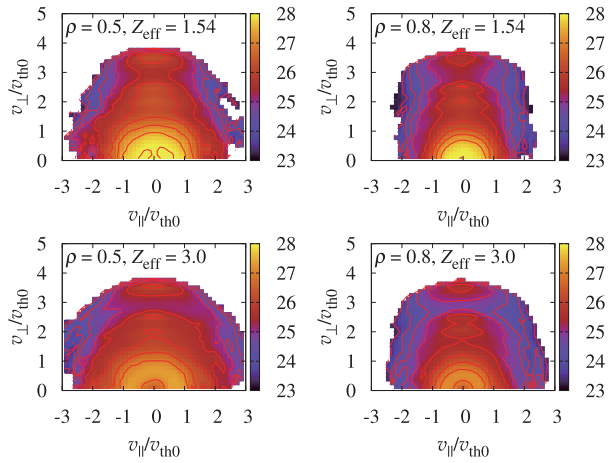

Fig. 2 Velocity space distribution of the NBI#5 fast ions for $Z_{\rm eff}$ = 1.54 (top) and $Z_{\rm eff}$ = 3.0 (bottom).

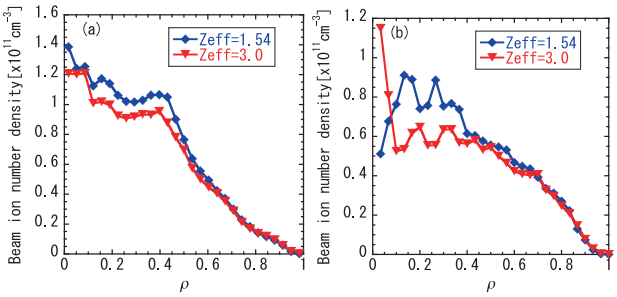

Fig. 3 Radial distribution of the fast-ion density for (a) NB#1 and (b) NB#5 in plasmas with different $Z_{\rm eff}$ values. The birth profile is fixed to that of $Z_{\rm eff}$ = 1.54 case for both beam lines.

proton density decreases as the $Z_{\rm eff}$ increases. Therefore, the increase of the impurity ions tends to decrease the ionization by the charge exchange with protons in the NBI#5 case, where the charge exchange is the dominant ionization process (40 keV). On the other hand, for the beam energy greater than 80 keV, the impurity ion impact ionization becomes dominant. Thus we can see the opposite behavior of the birth rate as a function of the effective charge.

Next, we investigate the impurity effect on the slowing down of the fast ions. We fix the birth profiles and evaluated the fast ion distribution functions in the steady state to see the impurity effect on the slowing-down and remove it from the birth. Figure 2 shows the velocity distributions of the fast ions of NB#5 at ρ = 0.5 and 0.8 in the plasmas containing He^{2+} and C^{6+} with different $Z_{\rm eff}$ values calculated by using GNET. The birth profiles are fixed to that of the $Z_{\rm eff}$ = 1.54 case with the total absorbed power set at 1 MW. In Fig. 2, $v_{\parallel}$ and $v_{\perp}$ are the velocity parallel and perpendicular to the field line, respectively, and the normalizing $v_{\rm th0}$ is the ion thermal velocity at $T_{\rm i}$ = 3.0 keV. We can see the fast ions diffuse in velocity space owing to pitch-angle- and energy-scattering during slowing down. In addition, the pitch angle of the energetic fast ion with the velocity

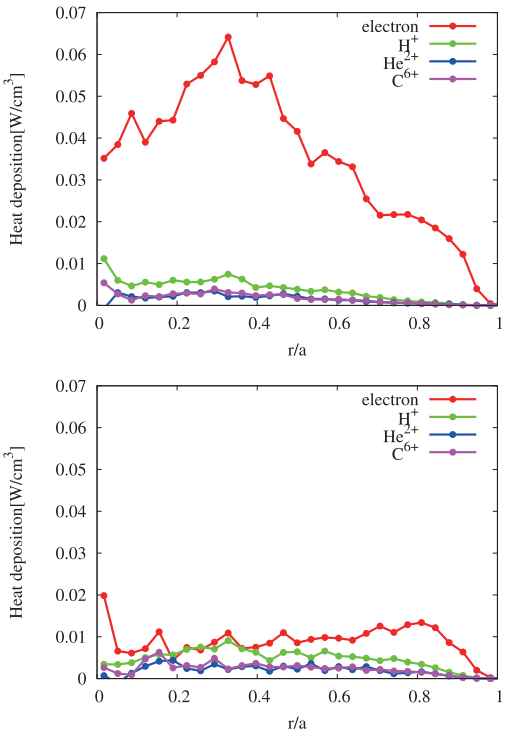

Fig. 4 Radial profile of the heat deposition of NBI#1 (top) and NBI#5 (bottom).

$v/v_{\rm th0} = \sqrt{v_{\parallel}^2 + v_{\perp}^2}/v_{\rm th0}$ = 1.0-4.0 broadens the in $Z_{\rm eff}$ = 3.0 case.

Figure 3 shows the radial distributions of the fast-ion density for (a)NB#1 and (b)NB#5. The impurity compositions are the same as that in Fig. 2 and the birth profiles are as in the $Z_{\rm eff}$ = 1.54 case for both beam lines. The decrease in the fast-ion number owing to the increase in $Z_{\rm eff}$ can be seen for both beam lines in Fig. 3. The results suggest that the radial transport of the fast ions increased owing to the enhancement of the pitch angle scattering by the impurity ions.

Finally, we investigate the impurity effect on the heat deposition profiles and the effective heat deposition. In this case, the change in birth profiles with impurity composition is considered. Figure 4 shows the radial profiles of the heat deposition per unit volume where the background ion species consist of 60% H^+, 30% He^{2+}, and 10% C^{6+} in number density. The total absorbed power of neutral beam is set to 1 MW for both NBI#1 and NBI#5 cases. Figures 5 and 6 show the volume-integrated heat deposition of NB#1 and NB#5, respectively, divided by the density at the center for electrons and total ion species. The port-through power is set to 1 MW and the shine-through loss fraction is taken into account by weighting the fast-ion birth rates for both beam lines. Figure 5 shows that the heat deposition of NB#1 per particle is effectively increased by the impurity ions. The increment of the heat deposition of NBI#1 per unit increment in $Z_{\rm eff}$ is about 15% for electrons and 28% for ions. In the NBI#5 case, on the other hand, the heat

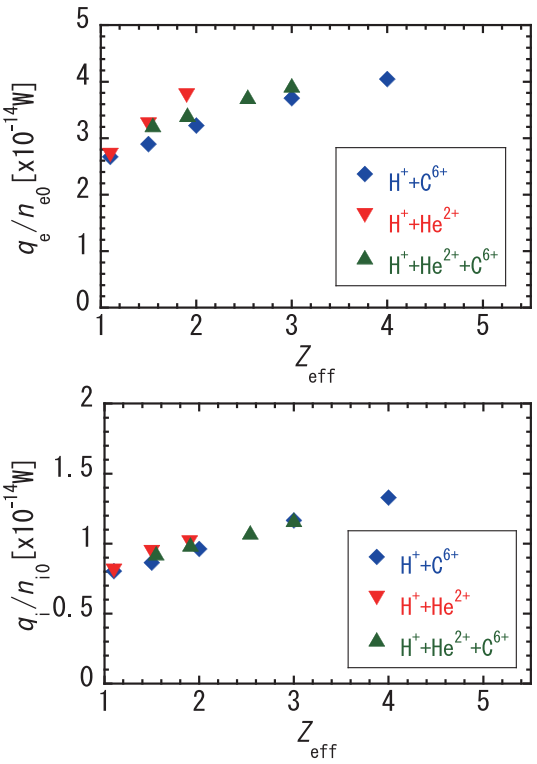

Fig. 5 Volume-integrated heat deposition per electron (top) and per ion (bottom) in the NBI#1 case.

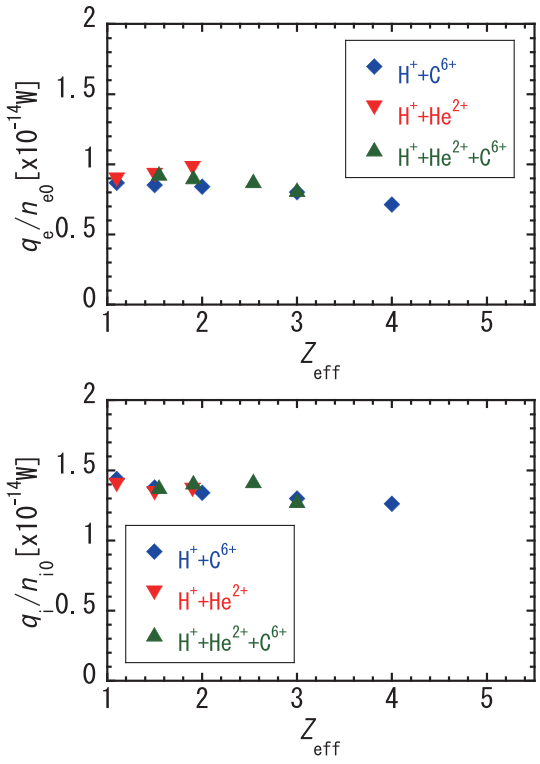

Fig. 6 Volume-integrated heat deposition per electron (top) and per ion (bottom) in the NBI#5 case.

deposition per particle tends to decrease with Z_{eff}, with the exception of electron heating in the He^{2+} plasma.

4. Summary

We have studied the effect of the impurity ions on the heat deposition of NBI heating using the HFREYA and GNET codes in LHD plasmas. We evaluated the fast-ion birth profile by using the HFREYA code. As Z_{eff} goes up, the fast-ion birth rate increases in the NB#1 (beam energy 180 keV) case and decreases in the NB#5 (beam energy 40 keV) case. We solved the drift kinetic equation of the fast ions in five-dimensional phase space using the GNET code. The impurity ions enhance the pitch angle scattering of the fast ions and degrade the fast-ion confinement. The simulation results also showed that, as the Z_{eff} increases, the net heat deposition per particle effectively increases in the NB#1 case, whereas it slightly decreases with in the NB#5 case.

In the future, we will study the impurity effect with the GNET-TD code [6] and perform time-dependent NBI heating simulations of the time-evolving plasma in the high-T_i experiment.

[1] H. Takahashi *et al.*, Nucl. Fusion **53**, 073034 (2013).
[2] K. Nagaoka *et al.*, Nucl. Fusion **51**, 083022 (2011).
[3] K. Ikeda *et al.*, J. Plasma Fusion Res. SERIES **9**, 88 (2010).
[4] S. Murakami *et al.*, Nucl. Fusion **40**, 693 (2000).
[5] S. Murakami *et al.*, Nucl. Fusion **46**, S425 (2006).
[6] H. Yamaguchi *et al.*, Plasma Fusion Res. **8**, 2403099 (2013).
[7] S. Murakami *et al.*, Fusion Technology **27**, Suppl. S 256 (1995).
[8] R.K. Janev *et al.*, Nucl. Fusion **29**, 2125 (1989).
[9] A.H. Boozer and G. Kou-Petravic, Phys. Fluids **24**, 851 (1981).